Algorithm to derive exact exchange-correlation potentials from correlated densities in atoms

K. Peirs,* D. Van Neck,† and M. Waroquier
Laboratory of Theoretical Physics, Ghent University, Proeftuinstraat 86, B-9000 Gent, Belgium
(Received 19 July 2002; revised manuscript received 1 October 2002; published 23 January 2003)

A simple algorithm is presented to derive accurately the exchange-correlation potential in the density functional theory (DFT) from the electron density. The method, which can be used with any physically acceptable density as input, is applied here to the densities in atoms obtained from high-level Green's function calculations. The resulting potentials show the correct asymptotic behavior and the characteristic intershell peaks. We illustrate the possible use of these potentials in fitting procedures for new functionals, by investigating the HCTH functional [F. A. Hamprecht, A. J. Cohen, D. J. Tozer, and N. C. Handy, J. Chem. Phys. **109**, 6264 (1998)]. The potentials derived from Green's function one-body densities provide a microscopic foundation for present-day functionals in DFT, and may therefore be helpful in the ultimate goal of constructing functionals on a fully *ab initio* basis.

DOI: 10.1103/PhysRevA.67.012505 PACS number(s): 31.15.Ew, 31.25.−v

I. INTRODUCTION

The density functional theory (DFT) for electronic systems is found on a one-to-one mapping of the external potential acting on a system of N electrons and the electron density in the ground-state configuration (Ref. [1]; see, also, e.g., Refs. [2] or [3]). In this way, the density can be regarded as the key observable, from which all other properties of the many-body systems are derived. In practical DFT calculations, the density is determined by solving Schrödinger-like equations for single-particle orbitals, the Kohn-Sham equations [4]. The Kohn-Sham method, however, depends on an external input, namely the exchange-correlation (xc) potential, in which one tries to fold the effects of the electron-electron interaction into a one-body potential. Within the DFT formalism, this potential is defined as the functional derivative of the xc functional. Due to this phenomenological input, DFT is computationally fast, but the accuracy of its predictions largely depends on the quality of the xc potential used in the calculation. Since DFT proves only the existence of a unique and universal xc potential, but does not give clues on how to construct it, a large number of xc functionals have been proposed on semiempirical grounds.

Although these functionals are quite successful, they are constructed by a fit to experimental data, which is less satisfying from a theoretical point of view. As present-day applications of DFT become more challenging, there is a growing interest in more advanced functionals. Therefore, a more systematic way to improve functionals is desireable from both a theoretical as well as a practical viewpoint.

Many commonly used xc functionals describe correctly only the region in space where the electron density is substantial. However, the asymptotic behavior of the corresponding potential $(-1/r)$ can be erratic (e.g., the LDA [5,6] or BLYP functional [7,8]). This is not problematic when only the total energy is to be predicted since the asymptotic region is not important for this observable. Yet, other quantities such as atomic electron affinities and properties related to the response to an electromagnetic field (e.g., polarizabilities) depend on the asymptotic behavior of the density in a crucial way [9]. Several efforts have been made to find systematic tools to improve the functionals in the asymptotic region. One way is to include (fractions of) exact exchange in the functionals, while fitting the parameters of the functional to energetic data only (see Refs. [10–13]). Another route, which is also followed in this paper, is to include not only energetics in the fit but also xc potentials derived in an *ab initio* approach (see, e.g., Ref. [14]). The idea is to calculate the one-body electron density using a very accurate method such as Monte Carlo, configuration interaction, coupled-cluster or Green's function techniques. In these methods, the amount of correlations embodied in the electron density can be increased systematically e.g., by taking into account more interacting configurations, which of course increases the numerical cost. It has even been suggested to use experimental electron densities [15].

In previous papers, we performed calculations using self-consistent Green's function theory for atomic systems ([16–18]). More particularly, we solved the Dyson equation self-consistently up to second order in the two-body interaction. The resulting one-body density extracted using this method incorporates a major part of the correlations present in the atomic systems. We then need an algorithm to find the exact xc potential that DFT would require to decribe the same atomic density.

This is the so-called inversion problem and over the years several algorithms to solve this problem have been developed (see, e.g., Refs. [19–29]), though they are sometimes restricted to a few small systems like helium, beryllium, and neon atoms. Amongst the more general schemes we mention in particular the density response scheme of Refs. [22,27], and the method of Zhao, Morrison, and Parr (ZMP, see, Ref. [28]). The former technique generates the Kohn-Sham potential by solving an integral equation for the inverse response function of the Kohn-Sham system, while in the latter the noninteracting kinetic energy is minimized under the restriction that the Kohn-Sham density equals the input density.

*Corresponding author. Email address: karel.peirs@rug.ac.be
†Corresponding author. Email address: dimitri.vanneck@rug.ac.be

These methods have a solid physical foundation, but they are rather intricate and can be difficult to implement in a numerically stable way.

In this paper, we tackle the inversion problem in coordinate space using a new scheme, that is simple, numerically robust and applicable to any atomic input density. The basic principles underlaying the scheme are quite general and we therefore expect the scheme to work for systems without spherical symmetry as well. The procedure, which uses an iterative local update of the exchange-correlation potential, is similar to the procedure proposed in Ref. [25] but seems to be numerically more stable. As indicated above, we will apply this algorithm to electron-densities obtained from Green's function calculations. The potentials generated by the scheme show the correct asymptotic behavior and the characteristic intershell peaks.

We can then use these potentials in fitting procedures for existing or new functionals, along with energetic data resulting from the same Green's function calculation. In this way, a microscopic study of current functionals can be performed, providing an *ab initio* basis for these functionals. This may result in model potentials with e.g., improved asymptotic behavior such that some properties, like polarization quantities, are predicted with larger accuracy. Efforts along this path can lead to more fundamental guidelines to derive functionals, thereby hopefully increasing the predictive power of DFT. We illustrate this procedure in a preliminary study of a recent functional proposed by Hamprecht *et al.* (the HCTH functional, see, Ref. [30]).

The outline of this paper is as follows. In Sec. II, the inversion algorithm is presented that determines the xc potential corresponding to a given input one-body density. Though this section is mainly numerical in nature, we point out the underlaying physical principles of the algorithm where possible. In Sec. IV, we discuss the potentials found for some closed-shell atoms (He, Be, Ne, Mg, and Ar) and open-shell atoms (B, C, N, O, and F) using the densities as derived from our self-consistent Green's function scheme. An example of the microscopic analysis of functionals is given in Sec. V, where we present some preliminary results of our study on the HCTH functional. Finally, a survey of the key features in this paper is given in Sec. VI.

II. INVERSE-PROBLEM ALGORITHM

The algorithm will be presented in a spin-restricted formalism: the spin-polarized version of the expressions can be found by simply adding the spin-index σ. Atomic units are used throughout the paper.

For a given N-electron input density $\rho_{ref}(\mathbf{r})$, the inversion problem consists of determining the unique local potential $v_s(\mathbf{r})$ that generates this density through the Kohn-Sham (KS) equations. Stated otherwise, we must have that

$$\rho_{ref}(\mathbf{r}) = \rho_{KS}(\mathbf{r}) = \sum_{i=1}^{N} |\phi_{KS,i}(\mathbf{r})|^2, \tag{1}$$

where the Kohn-Sham orbitals in Eq. (1) are lowest-energy solutions of

$$[-\tfrac{1}{2}\nabla^2 + v_s(\mathbf{r})]\phi_{KS,i}(\mathbf{r}) = \epsilon_{KS,i}\phi_{KS,i}(\mathbf{r}). \tag{2}$$

In general, the effective potential of the KS system reads

$$v_s(\mathbf{r}) = v_0(\mathbf{r}) + \int d^3r' \frac{\rho_{KS}(\mathbf{r}')}{|\mathbf{r}-\mathbf{r}'|} + v_{xc}(\mathbf{r}), \tag{3}$$

and consists of the external potential v_0, the Hartree repulsion v_H, and the xc potential v_{xc}. We restrict our study to spherically symmetric atomic systems without additional external fields, i.e., $v_0(r) = -Z/r$, where Z is the atomic number. As a consequence, only the radial degree of freedom is relevant.

In our algorithm the inversion problem is solved using an iterative scheme. All terms in $v_s(\mathbf{r})$ that are known exactly are kept fixed over the iterations, i.e., only the xc potential is varied. The Hartree potential in Eq. (3) is evaluated using the input density $\rho_{ref}(r)$. We initialize the xc potential by means of the Dirac potential [6]:

$$v_{xc}^{(0)}(r) = -\left[\frac{3}{\pi}\rho_{ref}(r)\right]^{1/3}. \tag{4}$$

The Dirac potential provides a reasonable approximation for the exchange part, which is the dominant contribution to the xc potential.

Suppose that we have the xc potential of iteration n, then we solve the KS equations (2) corresponding to this potential in coordinate space and construct the KS electron density

$$\rho_{KS}^{(n)}(r) = \sum_{i=1}^{N} |\phi_{KS,i}^{(n)}(r)|^2. \tag{5}$$

The xc potential of the next iteration is found by applying the following correction:

$$v_{xc}^{(n+1)}(r) = v_{xc}^{(n)}(r) + \alpha r^{\beta}[\rho_{KS}^{(n)}(r) - \rho_{ref}(r)] + [\mathcal{I}_{KS}^{(n)} - \mathcal{I}_{ref}]f(r). \tag{6}$$

The last term in Eq. (6) contains the ionization energy $\mathcal{I}_{KS}^{(n)} = -\epsilon_{KS,ion}^{(n)}$, where $\epsilon_{KS,ion}^{(n)}$ is the energy of the highest occupied Kohn-Sham orbital in iteration n. The ionization energy $\mathcal{I}_{ref}$ determines unambiguously to the asymptotic behavior of the input density. Its role will be explained in the next paragraphs, along with the parameters α, β and the function $f(r)$.

With the update (6) for the xc potential, the KS equations are solved anew and this process is repeated until convergence. As the convergence criterion we impose a condition on the integrated density deviation,

$$4\pi \int dr r^2 |\rho_{KS}^{(n)}(r) - \rho_{ref}(r)| < \Delta, \tag{7}$$

where $\Delta = 10^{-5}$. For the open-shell inversion, the convergence condition is imposed on both spin densities separately and $\Delta_\sigma = 5 \times 10^{-6}$.

The effective KS potential v_s is only determined up to an additive constant by Eqs. (1) and (2), and can be fixed completely by the requirement that it vanishes at infinity. Due to

the fact that our initial guess (the Dirac potential) in Eq. (4) vanishes asymptotically, and due to the structure of the update scheme Eq. (6), this requirement is automatically fulfilled for the converged solution as well.

Any reasonable electron-density $\rho_{ref}(r)$ can be used as input in the algorithm. However, in order to get good asymptotic properties for the xc potential it is of course required that the input density itself has the correct exponential-type decay for a neutral atom [31],

$$\rho_{ref}(r) \sim e^{-2\kappa r} r^{2[(1/\kappa)-1]}, \tag{8}$$

where $\kappa = \sqrt{2\mathcal{I}_{ref}}$. Note that the ionization energy is in principle determined by the asymptotic region of the input density ρ_{ref}. We employed the highly correlated densities as obtained from our Green's function calculations (see, Refs. [16–18]), but the scheme can also be applied on densities found by other methods (e.g., quantum Monte Carlo calculations).

Let us now have a closer look at the update scheme in Eq. (6). The physical significance of the first correction term is that if the KS density of iteration n is larger than the reference density $\rho_{ref}(r)$ in some region in space, then the xc potential of the next iteration will become more repulsive in that region. In this way, the KS density of iteration $(n+1)$ should be closer to the input density.

In expression (6), the value of the (positive) parameters α and β is in general not crucial for the final converged form of the potential, but can have an important influence on the number of iterations required to reach convergence. The parameter α determines the overall weight of the local correction to the xc potential due to the difference between the KS and input density. The parameter β increases the weight of the large-r region, for which the correction would otherwise be very small.

We obtained convergence for α ranging from 0.5 to 3.5 a.u., while the value of β could be varied between zero and three, at least for all closed-shell atoms in this study. In the open-shell case, the tuning of the β parameter turned out to be more delicate, however, and it was found that its value should preferably be selected around $\beta \approx 2$ for B and C, while we obtained good results with $\beta \approx 1.5$ for N, O, and F.

It is clear that the first correction term is related to the idea that a minor change in the one-body density induces a linear-response reaction in the effective KS potential. The exact expression for this response is nonlocal,

$$\delta v_s(\mathbf{r}) = \int d\mathbf{r}' G^{-1}(\mathbf{r},\mathbf{r}')\,\delta\rho(\mathbf{r}'), \tag{9}$$

where the density response function of the KS system is defined as (for a closed-shell system)

$$G(\mathbf{r},\mathbf{r}') = 2 \sum_{i(occ.)} \sum_{j(unocc.)} \frac{\phi_i^*(\mathbf{r})\phi_j^*(\mathbf{r}')\phi_i(\mathbf{r}')\phi_j(\mathbf{r})}{\epsilon_i - \epsilon_j} + \text{c.c.} \tag{10}$$

Equations (9) and (10) have been used [22,23,27] to determine the effective KS potential by iteratively determining the inverse $G(\mathbf{r},\mathbf{r}')^{-1}$ of the response function. If the inverse G^{-1} is calculated using finite basis-set expansions for the potential and/or the KS orbitals, severe problems may arise [22,23]. These are not encountered in the grid-based method of Ref. [27], where it was found, however, that spurious oscillations appear in the converged potential if the input density does not have the correct asymptotic behavior. This indicates the sensitivity of the potential even to spatial regions where the density is very small, as will be further discussed in Sec. IV.

The second correction term in Eq. (6) is not strictly necessary to obtain convergence to an xc potential with correct asymptotic behavior (see Sec. IV). Without the second term, however, the highest occupied KS eigenvalue may be somewhat off the value for $\mathcal{I}_{ref}$ corresponding to the tail of the input density. This is due to the fact that in the asymptotic region, the first correction term (even with the extra factor r^{β}) is small, and a very large number of iterations would be required to obtain an accurate matching for the ionization energies. To alleviate this problem, we added the second term: it ensures that the absolute value of the energy of the highest occupied KS level coincides with the ionization energy $\mathcal{I}_{ref}$. The factor $f(r)$ in the second term has the following form:

$$f(r) = \theta(1-r)r^{\gamma} + \frac{\theta(r-1)}{r^{\delta}}. \tag{11}$$

The step functions $[\theta(x)]$ allow for a continuous transition between the two terms at a distance of one atomic unit. Again, the parameters γ and δ only affect the speed of convergence of the scheme; we only require their value to be positive. In our calculations, we used for $\gamma \approx 5$ for the closed-shell atoms and $\gamma \approx 1$ for the open-shell cases. The parameter δ can be taken $\delta \approx 3$ in all cases. Both parameters, however, can be varied within a wide range without affecting the final form of the converged potential.

III. NUMERICAL TEST OF THE SCHEME

The inversion algorithm as presented in the preceding section was first tested at the exchange-only level, using Hartree-Fock (HF) input densities calculated in coordinate space (see Refs. [16–18]). Note that the coordinate-space HF scheme automatically leads to the correct asymptotic behavior of Eq. (8). As an example, we show in Fig. 1 the effective exchange potential corresponding to the neon HF density. It is seen to be extremely close to the optimized effective potential exchange-only potential of Ref. [32], which is the local potential that generates orbitals which minimize the HF energy functional.

It is also interesting to compare the iterative procedure in Eq. (6) with that introduced by van Leeuwen and Baerends [25], henceforth called the LB scheme. The LB scheme for solving the inversion problem uses a different local update,

$$v_{el}^{(n+1)}(r) = U^{(n)}(r) v_{el}^{(n)}(r), \tag{12}$$

$$U^{(n)}(r) = \frac{\rho_{KS}^{(n)}(r)}{\rho_{ref}(r)}, \tag{13}$$

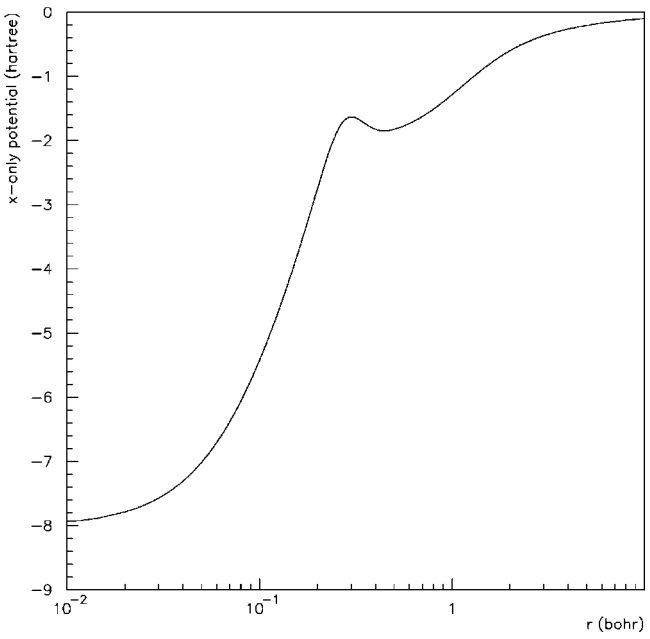

FIG. 1. Exchange-only potential generated from the neon Hartree-Fock density in Fig. 3.

where $v_{el}(r)=v_H(r)+v_{xc}(r)$ the electron-electron part of the KS potential.[1] The update factor $U(r)=\rho_{KS}(r)/\rho_{ref}(r)$ must be kept within reasonable bounds, e.g., by imposing [25]

$$1-\epsilon \leqslant U(r) \leqslant 1+\epsilon, \tag{15}$$

where $\epsilon \sim 0.05$, or by considering [26]

$$U(r)=\frac{\rho_{KS}(r)+a}{\rho_{ref}(r)+a}, \tag{16}$$

where $a \sim 0.5$ atomic units.

Note that a local update scheme in terms of a multiplicative factor with fixed sign [like the ratio of the nth iteration density and the target density in Eq. (13)] is problematic in the sense that it cannot change the local sign of the unknown potential from its initial estimate. While this hardly matters for electron systems—one can isolate the v_{el} part which has a fixed sign—it can be unworkable in other problems, e.g., in nuclear physics. So on general grounds an iterative scheme like Eq. (6), where the unknown potential can change its local sign during iterations, is to be prefered.

[1]In the original sciheme appearing in Ref. [25],

$$v_s^{(n+1)}(r)=\frac{\rho_{KS}^{(n)}(r)}{\rho_{ref}(r)}v_s^{(n)}(r), \tag{14}$$

obviously some printing error has occurred; it is defined in the unstable direction since the total KS potential $v_s(r)$ is usually negative. The stable direction would involve the local update factor $\rho_{ref}(r)/\rho_{KS}^{(n)}(r)$. In later papers by the Amsterdam group and coworkers it is clear that they advocate updating, according to Eq. (13), the electron-electron part of the KS potential only, which is a positive quantity.

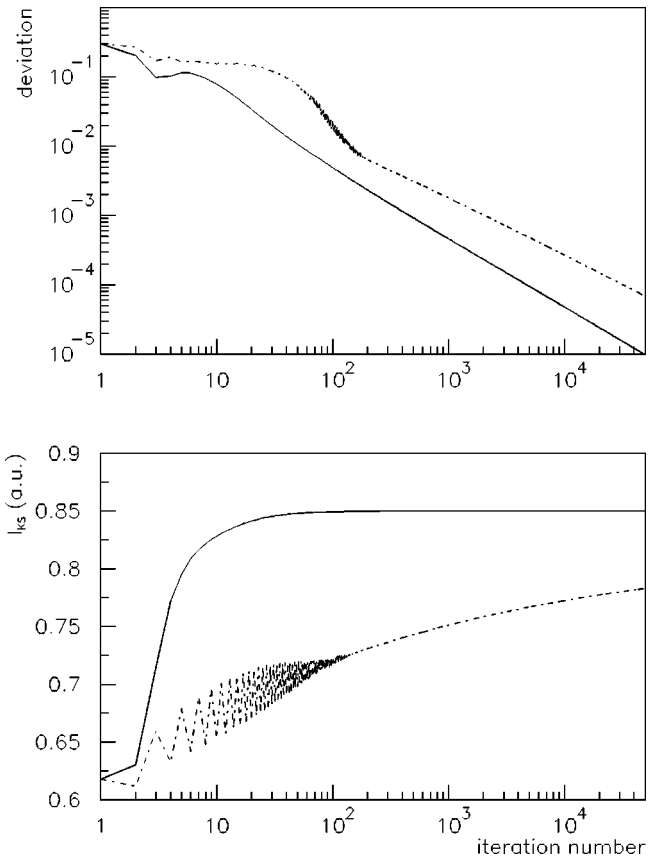

FIG. 2. Comparison of convergence properties of the present method in Eq. (6) and the LB method of Eqs. (12) and (13). The neon HF density was used as input. Full line: present method. Dot-dashed line: LB method. Upper panel: integrated density deviation of Eq. (7) versus iteration number. Lower panel: KS ionization energy (in atomic units) versus iteration number.

Another practical remark is that the LB method seems to be much more sensitive to the initial estimate for the xc potential, e.g., using the Dirac expression (4) we failed to achieve convergence for the neon Hartree-Fock density. We did obtain convergent results using (see Ref. [27]) an initial estimate

$$v_{xc}^{(0)}(r)=-\left[\frac{3}{\pi}\rho_{ref}(r)\right]^{1/3}+2\epsilon_x^B(\rho_{ref}(r),|\nabla\rho_{ref}(r)|), \tag{17}$$

where ϵ_x^B is the Becke [7] gradient correction to the exchange energy density; the latter term imposes the correct asymptotic $-1/r$ behavior of the initial estimate. Note that in the present scheme (6) this behavior is built up automatically during iterations, even with an initial estimate like Eq. (4) which is exponentially decaying.

In the upper panel of Fig. 2 we compare, for the case of the neon HF density, the convergence speed of the density deviation in Eq. (7) for the LB and the present scheme. For the LB scheme expression (16) was used with $a=3$ a.u.; smaller values of a, or the use of expression (15), both led to instabilities in the recursion scheme. For the present scheme (6) parameter values $\alpha=3.5$, $\beta=1$, $\gamma=5$, $\delta=3$ have been

taken. In both cases the initial estimate (17) was used. The present scheme seems to converge faster for this case. Moreover, the ionization energy consistent with the input HF density for Ne, $I_{ref}=0.850$ a.u., is reached very rapidly, as can be seen in the lower panel of Fig. 2. The LB scheme yields an ionization energy which is approaching the correct one, but convergence is slow.

IV. RESULTS

The inversion algorithm was next applied at the full exchange *plus* correlation level using input densities resulting from Green's function calculations in which Dyson's equation is solved self-consistently up to second-order in the two-body interaction. As was demonstrated in Refs. [16–18], this so-called Dyson(2) scheme incorporates the most important correlations in many-electron systems, providing a good reproduction of e.g., ionization energies, electron affinities, and total energies.

The Dyson(2) scheme uses a HF basis set, which is constructed by solving the HF equations in coordinate space [Dyson(1) scheme]. Inherent to the method is a discretization of the continuum part of the energy spectrum by adding a parabolic potential wall to the HF hamiltonian. This wall is switched on only at a large distance (larger than approximately three a.u.) from the nucleus, where the one-body density is already in its asymptotic regime. Although the energetic aspects of the calculations are not influenced by this discretization scheme, the parabolic potential does affect the asymptotic region of the density. In view of the sensitivity of the inversion procedure an entirely correct asymptotic behavior is required, and therefore the Dyson(2) densities had to be corrected at large distances.

Near the point where the wall was applied, we imposed the correct asymptotic behavior as given in Eq. (8), where $\mathcal{I}_{ref}$ is the first ionization energy as predicted by the Dyson(2) scheme. Because small errors in the density are greatly magnified by the inversion procedure, it is crucial to apply this correction in a very smooth way by ensuring that the first, second, and third derivative of the density are continuous in the extrapolation region. This sensitivity is not intrinsic to our scheme but has also been observed in other inversion algorithms (see Ref. [33]).

The extrapolation procedure sketched above is illustrated in Fig. 3, where the HF, Dyson(2), and corrected Dyson(2) densities for neon are shown. The asymptotic regimes of the HF and Dyson(2) densities differ because the ionization energy as predicted by the two schemes is not equal.

The algorithm of Sec. II is applied to a number of light atoms: the closed-shell systems He, Be, Ne, Mg, and Ar and the open $2p$ shell atoms B, C, N, O, and F. We reached fast convergence [according to the criterion Eq. (7)] for each atom in our study. This means that we have found a basis-set free representation of the KS xc potential, and that we obtained the unique potential corresponding to our Dyson(2) input densities, up to some arbitrary constant. Note that it is not guaranteed that the scheme will converge for an arbitrary input density, since in principle there may be densities that are not noninteracting v-representable [25].

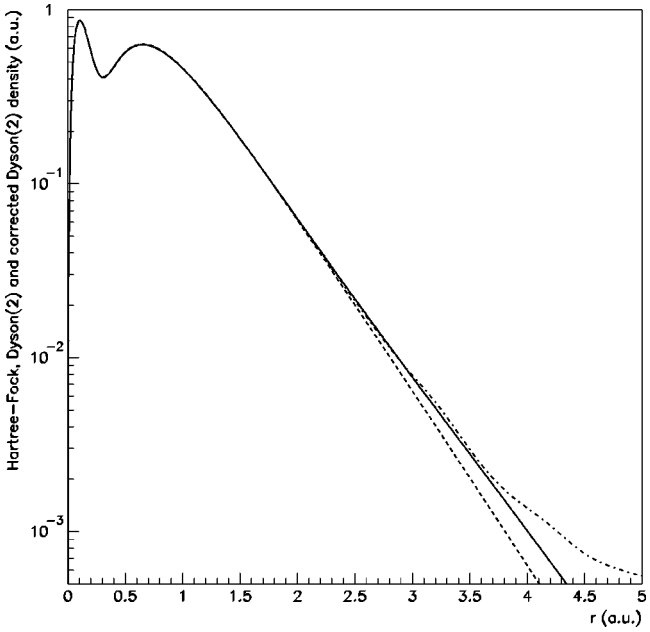

FIG. 3. Hartree-Fock (dashed), Dyson(2) (dot-dashed), and corrected Dyson(2) (full line) density for neon.

At convergence, we not only reproduce the input density in an accurate way, but also the highest occupied KS eigenvalue coincides with the Dyson(2) ionization energy (with an accuracy of about 10^{-7} a.u. or better). Moreover, the potentials show the correct asymptotic behavior $\sim -1/r$. This feature is not imposed on the potential by hand, but is generated automatically, probably due to the feedback mechanism between the update of the potential, the KS orbitals, and the physical input density having the correct large-r behavior of Eq. (8). Let us consider an electron of a neutral atom at a very large distance from the nucleus. As is well-known, the electron experiences a nuclear potential, shielded by the other $(Z-1)$ electrons. The influence of the nucleus on the electron is expressed by $-1/r$. The nuclear potential $-Z/r$ and the Hartree field $\int d^3r' \rho(\mathbf{r}')/|\mathbf{r}-\mathbf{r}'|$, however, cancel each other at large distances, such that the residual $-1/r$ potential must be generated by the xc potential.

In Figs. 4–6, we group the xc potentials from our scheme for the closed-shell systems. The upper part shows the potential itself, while the lower part involves $rv_{xc}(r)$ in order to illustrate in a more transparent way the correct asymptotic behavior of the potential. For comparison, we also include a high-level xc potential for He obtained by Umrigar and Gonze [34], as well as quantum Monte Carlo (QMC) results for Be and Ne obtained by the same authors [35] and by Filippi, Gonze and Umrigar [33]. These high-level potentials have also been used in Refs. [36–38]. It is clear that our results agree very well with these potentials, especially in the case of helium. There our potential only differs from the high-level potential at the origin [in the lower part of Fig. 4 with $rv_{xc}(r)$ the two curves practically coincide].

The spin-up and spin-down potentials for the open-shell B, C, N, O, and F atoms are displayed in Figs. 7–11. Note that the spin-up and spin-down potentials for F (Fig. 11) are

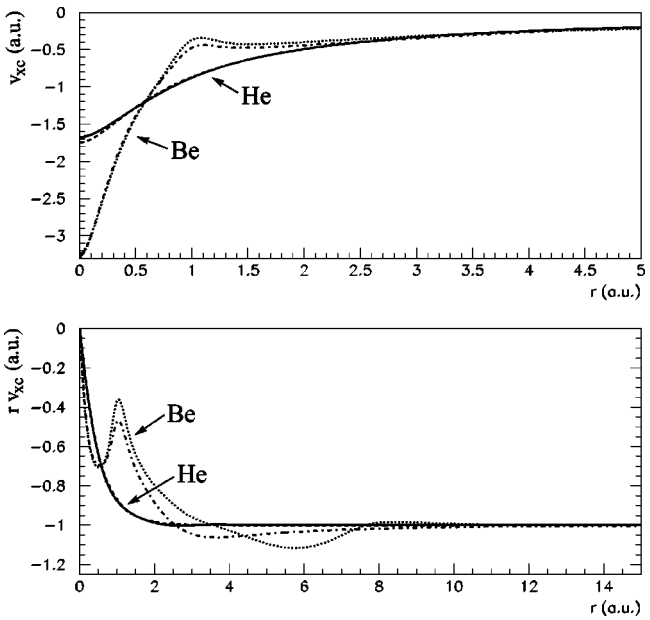

FIG. 4. Exchange-correlation potentials $v_{xc}(r)$ (upper part) and $rv_{xc}(r)$ (lower part) for He and Be as obtained in this work and in Refs. [34,39]: full line, He (this work); dashed line, He (high-level calculation [34]); dotted line, Be (this work); dot-dashed line, Be (QMC [39]).

very alike, as the atom approaches a closed-shell configuration.

A characteristic feature, present in all xc potentials, is the appearance of the intershell peaks. They can be partly related to a jump of the exchange hole from one shell to another if the reference position crosses the border region between the two shells (see Refs. [41–43]).

The lower part of each figure displaying $rv_{xc}(r)$ systematically reveals the correct asymptotic behavior of the xc potential. Also, we find that the xc potential has a finite value at the origin, as was already suggested by Morrison and Zhao [40]. The $rv_{xc}(r)$ curves provide a very sensitive look at the long-range behavior of the xc potentials. Comparing, for the case of Ne in Fig. 5, the present result with the QMC result it is clear that two spurious extrema appear in the potential based on the Dyson(2) density. Such artificial structure is present for the xc potentials of the other atoms as well, and is related to the extrapolation procedure in the asymptotic region of the density. Though we take care to extrapolate in a

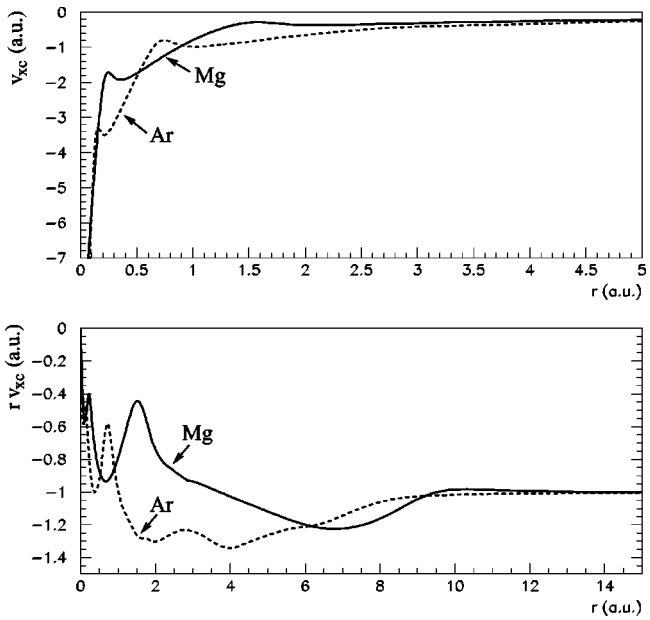

FIG. 6. Potentials of present work for Mg (full line) and Ar (dashed) [$v_{xc}(r)$ (upper part) and $rv_{xc}(r)$ (lower part)].

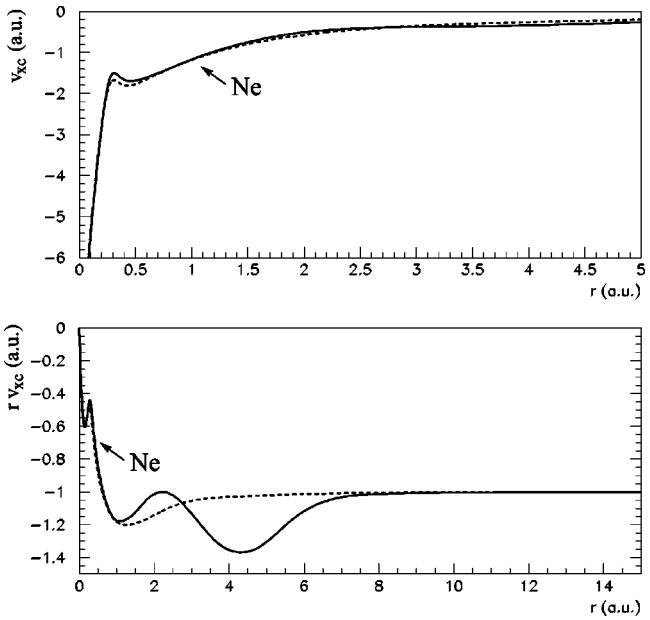

FIG. 5. Potentials for Ne [$v_{xc}(r)$ (upper part) and $rv_{xc}(r)$ (lower part)]: full line is this work, dashed line is the QMC potential [39].

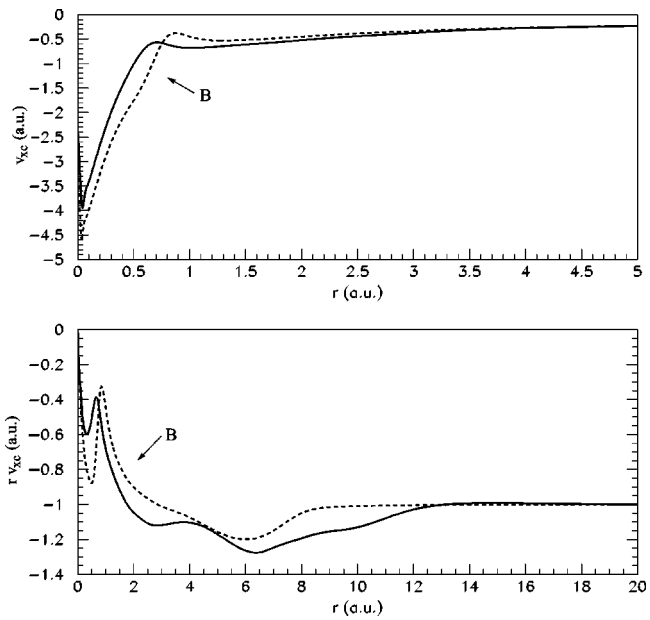

FIG. 7. Exchange-correlation potentials $v_{xc}(r)$ (upper part) and $rv_{xc}(r)$ (lower part) of present work for B: majority spin in full line, minority spin in dashed line.

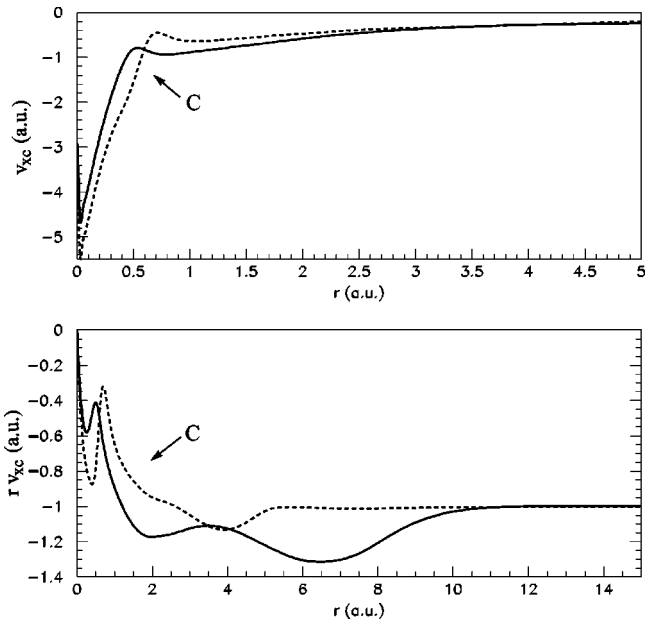

FIG. 8. Exchange-correlation potentials $v_{xc}(r)$ (upper part) and $rv_{xc}(r)$ (lower part) of present work for C: majority spin in full line, minority spin in dashed line.

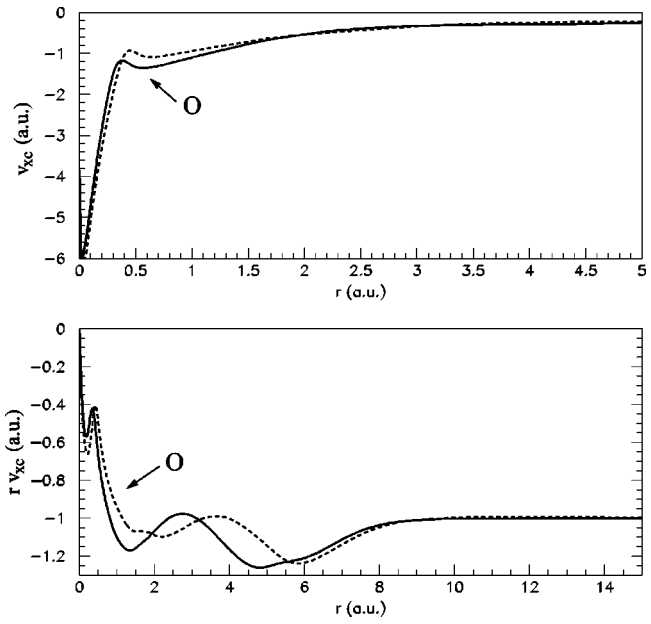

FIG. 10. Exchange-correlation potentials $v_{xc}(r)$ (upper part) and $rv_{xc}(r)$ (lower part) of present work for O: majority spin in full line, minority spin in dashed line.

smooth manner, the procedure still affects (mildly) the xc potential near the extrapolation point. The effect is entirely due to imperfections in the extrapolated Dyson(2) input density, and not to the used inversion procedure, since we do not encounter it when we use HF input densities or the QMC neon density, communicated to us by Gonze [39]. This observation is similar to the appearance of spurious oscillations in the xc potential reported by Schipper, Gritsenko, and Baerends [27] when a Gaussian-type input density is used.

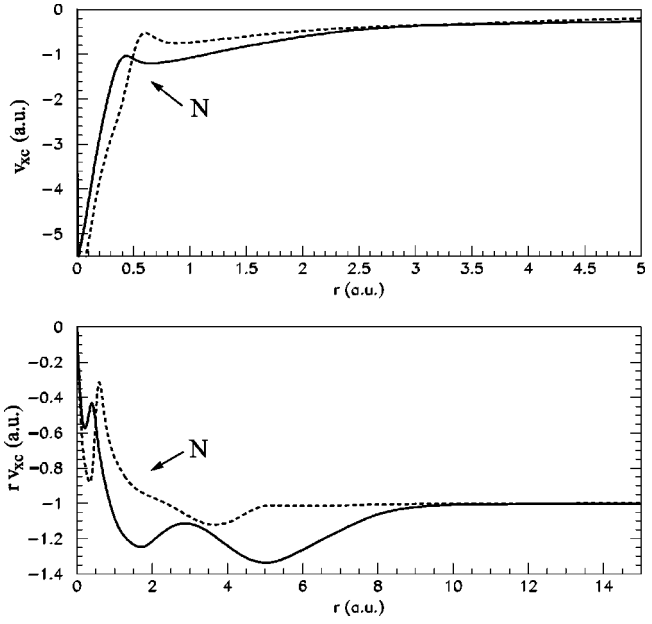

FIG. 9. Exchange-correlation potentials $v_{xc}(r)$ (upper part) and $rv_{xc}(r)$ (lower part) of present work for N: majority spin in full line, minority spin in dashed line.

Here we impose on the input density the correct asymptotic behavior by extrapolation, leading to less pronounced and more localized oscillations near the extrapolation point.

Since the xc potential constructed with the presented algorithm results in an almost perfect reproduction of the input density, one may assume that all correlations involved in the density are also present in the xc potential. Therefore, the xc potentials obtained in the present study incorporate all

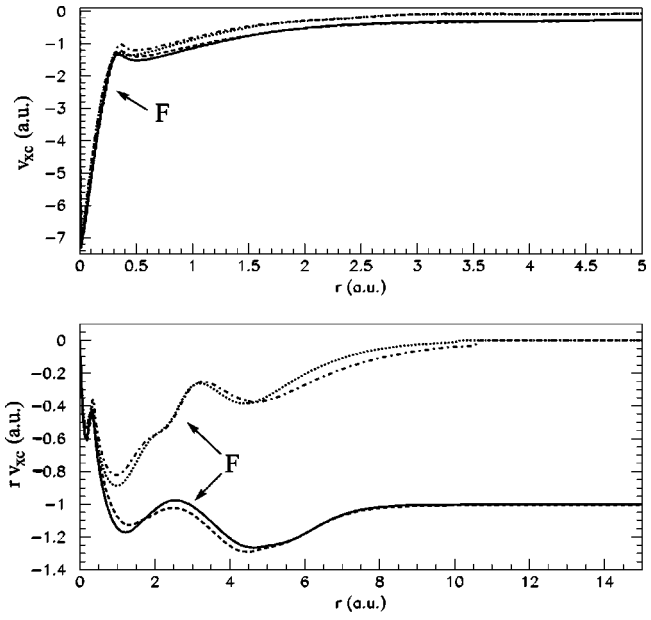

FIG. 11. Exchange-correlation potentials $v_{xc}(r)$ (upper part) and $rv_{xc}(r)$ (lower part) for F: inversion scheme, majority spin of F (full); minority spin of F (dashed); HCTH functional with new exchange parameters, majority spin of F (dotted); and minority spin of F (dot-dashed).

Dyson(2) correlations, i.e., all correlations of the self-consistent Green's function scheme up to second order in the Coulomb interaction.

The generated xc potentials can be used in a variety of applications. In this paper, we consider the use of these xc potentials in a fitting procedure for an existing functional parametrization. The resulting parameter set can then be considered to be derived on a fully microscopic basis, i.e., without fitting to experimental data. This will be illustrated in the following section with some preliminary results.

V. USE OF THE POTENTIALS IN FITTING PROCEDURES

As mentioned in the introduction, the asymptotic region of the xc potential becomes more and more prerequisite in present-day applications of DFT. Including exact xc potentials in the fitting procedure for a model functional provides more detailed information on how the model potential should behave, which may result in improved asymptotic densities and more accurate optimized geometries. It should be noted that good structural predictions can also be obtained by including exact exchange in the functional, and fitting to energetic data solely.

As far as aymptotics is concerned, there are actually two problems with current popular xc functionals. First, the majority of the potentials decreases in an exponential way instead of as $-1/r$. This means that the potentials are less attractive than the exact one at large r. There have been a number of efforts to correct the behavior at large r. One of the first attempts was made by van Leeuwen and Baerends [25], who introduced a model potential with an improved asymptotic behavior. However, the potential cannot be derived as the derivative of a functional and provides a less accurate description of the region close to the nucleus.

The second problem is more of an abstract nature and concerns the extension of DFT that also deals with systems consisting of a fractional number of electrons. As indicated in Sec II the exact KS potential, defined as the local potential that generates the exact density through Eqs. (1) and (2), is only determined up to an additive constant. If one considers an ensemble-based extension of DFT and its KS formulation to noninteger electron number one can also define the KS potential as the functional derivative of the underlying exact xc energy functional, valid for integer and noninteger electron number. This seemingly removes the freedom of the additive constant by relating it to the total energy, but this is not correct: at integer electron number the derivative is ill defined, and the exact KS potential jumps by a system-dependent constant when taking the limit to an integer from the electron-deficient or electron-abundant side (the so-called derivative discontinuity, [44]). So at integer electron number the exact KS potential is again defined up to an additive constant, and it can be shown (see, e.g., Refs. [9,14]) that an xc potential which vanishes asymptotically corresponds to taking the limit from the electron-deficient side. Earlier discussions on this topic can be found in Ref. [31] (asymptotic behavior of xc potentials) and [45] (constant shift of the potential). None of the currently implemented functionals describes this derivative discontinuity, and it is doubtful whether any analytical formulation will be able to include this phenomenon.

It was observed by Tozer and Handy [9,14] that generalized gradient approximation (GGA) functionals could more easily be fitted to exact xc potentials if they left room for a system-dependent constant in the fit. They interpreted this as an indication that the GGA potentials represent an average of the electron-deficient and electron-abundant limit of the exact xc potential. The same method was used by Hamprecht *et al.* [30], who fitted their model xc potential to both energetic data and accurate xc potentials obtained in the ZMP scheme. To include the derivative discontinuity to some extent in the functional, they allowed for a system-dependent constant shift of the input potentials. This shift does not enter the parameters of the functional explicitely, but has an indirect effect on the value of the parameters. However, the expansion defining the so-called HCTH functional leads to a potential that does not go to a constant but vanishes asymptotically.

In order to illustrate the use of the xc potentials resulting from our Dyson(2) calculations, we have made a refit of the HCTH functional. Currently, our training set only consists of the closed- and open-shell systems in our study, and results are therefore preliminary.

The HCTH xc functional can be written as

$$E_{xc}[\rho]=\sum_i c_i \int f_i(\rho_\uparrow,\zeta_\uparrow,\rho_\downarrow,\zeta_\downarrow)d\mathbf{r}, \tag{18}$$

where ρ_σ is the one-body spin density, $\zeta_\sigma=|\nabla\rho_\sigma|$, and the expansion functions f_i are described in Ref. [30]. In the HCTH functional, 15 functions f_i have been considered. The 15 expansion coefficients c_i are optimized in a least-squares fit with an objective function Ω that consists of two parts $\Omega=\Omega_V+\Omega_E$. The first part Ω_V involves the potentials

$$\Omega_V=\sum_\sigma \sum_A^{atoms} 4\pi \int dr r^2 \left[v_{input}^{A\sigma}(r)+k_A^\sigma - \sum_i c_i v_i^{A\sigma}(r)\right]^2 \rho_{A\sigma}^{2/3}(r), \tag{19}$$

where $v_{input}^{A\sigma}(r)$ is the xc potential for atom A as derived using our inversion algorithm, k_A^σ is the constant shift allowed for this potential, $v_i^{A\sigma}(r)$ is the potential derived from the function $f_i^A(r)$ by functional derivation with respect to $\rho_{A\sigma}(r)$, and $\rho_{A\sigma}^{2/3}(r)$ is an appropriate weighting factor.

The second term Ω_E in the objective function involves the energetic data,

$$\Omega_E=\sum_A^{atoms} w_A\left[E_{xc}^A-4\pi\sum_i c_i\int f_i^A(r)r^2dr\right]^2. \tag{20}$$

The xc energies E_{xc}^A can be determined from the well-known expression for the total energy in DFT,

TABLE I. Parameters of the HCTH functional: the first numerical column collects the original values, the next columns present the sets obtained using the Dyson(2) energies and xc potentials in the fit for different weights w_A of the energetic part of the objective function. Parameters are displayed which are obtained when varying only the exchange (x) parameters as well as varying both the exchange and the first three orders in correlation ($x+c$).

		x only			$x+c$		
Coefficient	Reference [30]	$w_A=10$	$w_A=100$	$w_A=1000$	$w_A=10$	$w_A=100$	$w_A=1000$
c_1	1.09320	1.089	1.089	1.078	1.091	1.059	1.051
c_2	0.222601				1.921	1.231	2.164
c_3	0.729974				−1.513	0.6931	1.029
c_4	−0.744056	−0.9258	−0.9038	−0.8424	−0.6457	−0.4957	−0.6129
c_5	−0.0338622				−0.6577	−0.3981	−0.4234
c_6	3.35287				0.2933	−2.679	−3.602
c_7	5.59920	6.956	7.057	8.599	7.414	6.818	6.719
c_8	−0.0125170				0.7298	−0.0519	−0.7304
c_9	−11.5430				−11.90	−11.258	−10.03
c_{10}	−6.78549	−9.693	−11.09	−19.67	−10.39	−9.601	−10.41
c_{11}	−0.802496						
c_{12}	8.08564						
c_{13}	4.49357	7.168	8.443	17.42	7.746	7.119	8.869
c_{14}	1.55396						
c_{15}	−4.47857						

$$E_{xc}[\rho_A]=E_{0(A)}-\sum_{i(occ)}\epsilon_{KS,i}+J[\rho_A]+4\pi\sum_{\sigma}\int drr^2 v_{input}^{A\sigma}(r)\rho_{A\sigma}(r), \tag{21}$$

where $E_{0(A)}$ is the ground-state energy of system A corresponding to the one-body density as determined in our Green's function calculations, while the KS eigenvalues $\epsilon_{KS,i}$ are generated by the inversion scheme. Furthermore, $J[\rho_A]$ is the Hartree part of the two-electron interaction:

$$J[\rho_A]=\frac{1}{2}\int d\mathbf{r}d\mathbf{r}'\frac{\rho_A(\mathbf{r})\rho_A(\mathbf{r}')}{|\mathbf{r}-\mathbf{r}'|}, \tag{22}$$

with $\rho_A(\mathbf{r})=\rho_{A\uparrow}(\mathbf{r})+\rho_{A\downarrow}(\mathbf{r})$. The weights w_A in Eq. (20) balance the influence of the potential and energetic part in the fit.

In the original derivation of the HCTH functional [30], Hamprecht *et al.* introduced a self-consistent technique to determine the value of the system-dependent shift k_A^σ (see, also, Ref. [14]). In the present paper, we found no need for this procedure, but simply minimized the objective function with respect to both the functional parameters $\{c_i\}$ and the constant shifts $\{k_A^\sigma\}$. The conditions

$$\frac{\partial\Omega}{\partial c_i}=0;\quad \frac{\partial\Omega}{\partial k_A^\sigma}=0, \tag{23}$$

with $\Omega=\Omega_V+\Omega_E$ then lead to the least-squares equations

$$c_i:\quad \sum_{j=1}^{N_p}\mathcal{A}_{ij}c_j+\sum_{\sigma'}\sum_{M=1}^{N_a}\mathcal{A}_{iM_{\sigma'}}k_M^{\sigma'}=\mathcal{B}_i,\quad i=1,\ldots,N_p$$

$$k_A^\sigma:\quad \sum_{j=1}^{N_p}\mathcal{A}_{A_\sigma j}c_j+\sum_{\sigma'}\sum_{M=1}^{N_a}\mathcal{A}_{A_\sigma M_{\sigma'}}k_M^{\sigma'}=\mathcal{B}_{A\sigma},\quad A=1,\ldots,N_a, \tag{24}$$

where N_p and N_a are the numbers of parameters and atoms, respectively. The matrices $\mathcal{A}$ and $\mathcal{B}$ are given by

$$\mathcal{A}_{ij}=\sum_{\sigma'}\sum_{N=1}^{N_a}\left[\int drr^2 v_i^{N\sigma'}(r)v_j^{N\sigma'}(r)\rho_{N\sigma'}^{2/3}(r)+4\pi w_N\int drr^2 f_i^N(r)\int drr^2 f_j^N(r)\right],$$

$$\mathcal{A}_{iM_{\sigma'}}=-\int drr^2 v_i^{M\sigma'}(r)\rho_{M\sigma'}^{2/3}(r),$$

$$\mathcal{B}_i=\sum_{\sigma'}\sum_{N=1}^{N_a}\left\{\int drr^2 v_{input}^{N\sigma'}(r)v_i^{N\sigma'}(r)\rho_{N\sigma'}^{2/3}(r)+w_N E_{xc}[\rho_N]\int drr^2 f_i^N(r)\right\}, \tag{25}$$

for c_i and

$$\mathcal{A}_{A_\sigma j}=-\int drr^2\rho_{A\sigma}^{2/3}(r)v_j^{A\sigma}(r),$$

$$\mathcal{A}_{A_\sigma M_{\sigma'}}=\delta_{AM}\delta_{\sigma\sigma'}\int drr^2\rho_{A\sigma'}^{2/3}(r),$$

$$\mathcal{B}_{A\sigma}=-\int drr^2\rho_{A\sigma}^{2/3}(r)v_{input}^{A\sigma}(r), \tag{26}$$

TABLE II. Total energy for the closed-shell systems as predicted by the HCTH functional fitted to Dyson(2) quantities, for different values of the weight w_A in the fit. The last two rows respectively represent the total energies of the Dyson(2) scheme and the HCTH functional using the original parameters [30]. Also listed are results for Ca, which was not included in the training set. For Ca the Dyson(2) prediction is not available, and the energy is taken from a G3 calculation [46]. All results are in atomic units.

w_A	He	Be	Ne	Mg	Ar	Ca
10	−2.918	−14.662	−128.875	−199.973	−527.430	−677.468
100	−2.913	−14.651	−128.870	−199.970	−527.436	−677.480
1000	−2.913	−14.642	−128.879	−199.977	−527.432	−677.471
Dyson(2)	−2.899	−14.628	−128.888	−199.948	−527.422	−677.38450
HCTH	−2.918	−14.670	−128.962	−200.096	−527.678	−677.765

for k_A^σ.

In this preliminary fit we have substantially less fitting data (potentials and total energies of only ten atoms) than in the original parametrization by Hamprecht *et al.* [30], which involved basically the G2 training set. As a result some coefficients c_i tend to oscillate when allowed to vary freely in the fit. Therefore, we fixed the coefficients corresponding to the correlation terms in the expansion and applied a least-squares fit on the exchange parameters only (i.e., the coefficients c_1, c_4, c_7, c_{10}, and c_{13}) along with the system-dependent shifts k_A^σ. In Table I, we collect the original values of the parameters [30] together with our values for a few choices of the weights w_A. For simplicity, the weight is kept constant for all atoms. We also include the parameters obtained when allowing the exchange and the first three correlations orders to vary. We see that some parameters tend to differ substantially from the original parametrization, which we attribute to the reduced size of our training set. In the remainder of this paper, we will therefore report only results that are obtained with the parameter set in which merely the exchange parameters were optimized, while the correlation parameters were fixed on the original HCTH value.

The total energies as predicted using the HCTH functional (with the new exchange parameters of Table I) for the atoms of the training set and also for calcium are listed in Tables II and III. All results were obtained by solving the KS equations in coordinate space. The Dyson(2) energies used in the fitting procedure are given for comparison, as well as the outcome of a G3 calculation for calcium [46]. Note that this G3 calculation involves relativistic corrections, which can have a relatively important influence in an atom as calcium. These corrections were not included in our Dyson(2) study. The results using the original parametrization of the HCTH functional are listed as well. Mind, however, that the HCTH functional was fitted to experimental energies (amongst other quantities) and not to *ab initio* energies as in the present study.

In Tables IV and V the first ionization energies are presented along with the Dyson(2) ionization energies, and the constant shifts k_A of the atoms in our training set. In Table V, only the shift of the potential that corresponds to the spin which determines the first-ionization level is reported. The shift of the potential corresponding to the other spin polarization is of a similar value. The ionization energy is calculated according to Ref. [30]

$$\mathcal{I}_A = -\epsilon_{KS,ion}^A + k_A^\sigma. \tag{27}$$

Note that the ionization energies were not included in the fit. Nevertheless, we notice a good agreement with the Dyson(2) quantities. We observe that all shifts are positive and of the expected order of magnitude: theoretical considerations [14]

TABLE III. Total energy for the open-shell systems as predicted by the HCTH functional fitted to Dyson(2) quantities, for different values of the weight w_A in the fit. See also caption of Table II.

w_A	B	C	N	O	F
10	−24.631	−37.813	−54.557	−75.012	−99.669
100	−24.619	−37.801	−54.545	−75.003	−99.662
1000	−24.612	−37.797	−54.539	−75.006	−99.671
Dyson(2)	−24.600	−37.789	−54.543	−75.010	−99.678
HCTH	−24.645	−37.837	−54.593	−75.063	−99.737

TABLE IV. Upper part: closed-shell first-ionization energies $\mathcal{I}$ obtained with the HCTH functional, for the three sets of parameters corresponding to the weights $w_A = 10$, 100, 1000 in Table I, and the Dyson(2) ionization energy. Lower part: the constant shifts k_A of the potentials as determined by the fit, and the Dyson(2) value for the hardness. All results are in atomic units.

w_A	He	Be	Ne	Mg	Ar
			$\mathcal{I}$		
10	0.900	0.347	0.763	0.243	0.561
100	0.900	0.347	0.764	0.242	0.561
1000	0.902	0.346	0.766	0.243	0.563
Dyson(2)	0.906	0.320	0.763	0.274	0.585
			k_A		
10	0.321	0.144	0.274	0.075	0.184
100	0.321	0.143	0.272	0.073	0.183
1000	0.322	0.142	0.276	0.072	0.187
Hardness	0.453	0.160	0.381	0.137	0.293

TABLE V. Upper part: open-shell first-ionization energies $\mathcal{I}$ obtained with the HCTH functional and Dyson(2) ionization energy. Lower part: the constant shifts k_A^σ and Dyson(2) hardness. Only the shift of the potential that determines the ionization level is considered; the shift of the potential corresponding to the other spin polarization is about the same value. All results are in atomic units.

w_A	B	C	N	O	F
			$\mathcal{I}$		
10	0.302	0.409	0.529	0.494	0.619
100	0.302	0.409	0.529	0.495	0.620
1000	0.303	0.409	0.527	0.502	0.623
Dyson(2)	0.305	0.415	0.537	0.484	0.619
			k_A^σ		
10	0.162	0.190	0.226	0.246	0.253
100	0.160	0.189	0.225	0.244	0.251
1000	0.159	0.190	0.227	0.242	0.252
Hardness	0.149	0.185	0.268	0.226	0.246

indicate that this shift should be less than or equal to the hardness $(\mathcal{I}-\mathcal{A})/2$, where $\mathcal{A}$ is the electron affinity. Similar values of the shifts were obtained in Refs. [47,48] using other functionals. In Tables IV and V, we also give the predictions of the hardness in the Dyson(2) scheme. Since the closed-shell systems that were considered cannot bind an extra electron, the hardness equals half the ionization energy. This observation also holds for nitrogen. As was pointed out in Ref. [14], in the closed-shell case the shift should be less than the hardness, but equal to the hardness for the open-shell systems (see, also, Ref. [49]). We see that the fitting procedure indeed reveals this trend: the shift of the closed-shell systems is always less than the Dyson(2) hardness, while the shift of the open-shell systems is close to it. Of course, the fitting scheme does not reproduce the open-shell hardness exactly, but it is clear that the predicted shifts oscillate about the exact value. The larger deviation of the nitrogen value may be due to the fact that in this system one $2p$ spin orbital is assumed fully occupied, while the other one is completely empty. As pointed out by Perdew and Burke in Ref. [49], the constant shift equals the hardness whenever the ground state of the positive and negative ions can be obtained by removing or adding an electron in the same highest occupied KS level of the neutral atom. Since this is not the case in the spinunrestricted treatment of nitrogen, we can understand that the shift is below the hardness for this atom.

It was also mentioned in Ref. [14] that a shift which differs significantly from the hardness indicates that kinetic-energy effects give an important contribution to the derivative discontinuity of the xc potential of the corresponding atom. In future work we intend to study the correlation contribution to the DFT kinetic energy in more detail.

Apart from a discussion of the energetic predictions of the HCTH functional with the new exchange parameters, we can also compare the HCTH potential with those derived in the inversion scheme. This is illustrated for fluor in Fig. 11. For the new exchange parameters, we chose those in Table I corresponding to the weight $w_A=100$. The HCTH potential has the correct qualitative behavior in the region where the atomic density is substantial, but it breaks down in the asymptotic region.

VI. SUMMARY

In this paper, a scheme is proposed to derive the exact exchange-correlation potential in density functional theory from a high-level electron density. The proposed iterative scheme is easier to implement than other methods, such as the density-response scheme (see Refs. [22,27]) or the method of Zhao-Morrison-Parr [28], and numerically more stable than the related inversion method in Ref. [25]. We applied the scheme on some closed-shell atoms (He, Be, Ne, Mg, and Ar) and on a number of open-shell atoms from the second row of the periodic system (B, C, N, O, and F). The one-body densities we used as input to the algorithm were obtained from self-consistent Green's function calculations, and embody a large part of the correlations in many-electron systems. The resulting potentials were found to display the correct asymptotic behavior and showed the characteristic intershell peaks. In this way, we have found a basis-set free representation of the exchange-correlation potential in the Kohn-Sham formalism. Since the ideas that underlay the algorithm are quite general, we believe it to be applicable on molecules as well. Extension of the inversion scheme to diatomic molecules, where the cylinder symmetry still allows a coordinate-grid method, will be the topic of future work.

The generated xc potentials can be used in a variety of applications. One application, addressed in this paper, is the use of the xc potentials in fitting procedures for new functionals. The advantage of using potentials along with energetic data when fitting functionals is that the corresponding model exchange-correlation potential receives more accurate information on how the exact potential should behave, which may lead to more accurate optimized geometries. As an example we have used the energies from the Green's function calculations that produced the input densities employed in the inversion scheme, along with the corresponding potentials to refit the HCTH functional in a fully *ab initio* way. The correlations present in the Green's function calculation, which can be easily defined using Feynman diagrams, are embedded in the exchange-correlation potentials derived in our scheme. In this way, a microscopic basis can be provided for present-day functionals, which may lead to a more fundamental understanding of exchange-correlation functionals in density functional theory.

ACKNOWLEDGMENTS

We gratefully acknowledge Dr. X. Gonze for supplying us with the high-level exchange-correlation potentials for He, Be, and Ne. Also, we wish to thank Professor C.J. Umrigar and Dr. C. Filippi for the interesting communications. This study was supported by the Fund for Scientific Research–Flanders (FWO).

[1] P. Hohenberg and W. Kohn, Phys. Rev. **136**, B864 (1964).
[2] R. G. Parr; and W. Yang, *Density-Functional Theory of Atoms and Molecules* (Oxford University Press, Oxford, England, 1989).
[3] R. M. Dreizler and E. K. U. Gross, *Density Functional Theory* (Springer, Berlin, 1990).
[4] W. Kohn and L.J. Sham, Phys. Rev. **140**, A1133 (1965).
[5] F. Bloch, Z. Phys. **57**, 545 (1929).
[6] P.A.M. Dirac, Proc. Cambridge Philos. Soc. **26**, 376 (1930).
[7] A.D. Becke, Phys. Rev. A **38**, 3098 (1988).
[8] C. Lee, W. Yang, and R.G. Parr, Phys. Rev. B **37**, 785 (1988).
[9] D.J. Tozer and N.C. Handy, J. Chem. Phys. **109**, 10 180 (1998).
[10] A.D. Becke, J. Chem. Phys. **98**, 1372 (1993).
[11] A.D. Becke, J. Chem. Phys. **98**, 5648 (1993).
[12] A.D. Becke, J. Chem. Phys. **104**, 1040 (1996).
[13] A.D. Becke, J. Chem. Phys. **107**, 8554 (1997).
[14] D.J. Tozer and N.C. Handy, J. Chem. Phys. **108**, 2545 (1998).
[15] A. Holas and N.H. March, Phys. Rev. A **44**, 5521 (1991).
[16] D. Van Neck, K. Peirs, and M. Waroquier, J. Chem. Phys. **115**, 15 (2001).
[17] K. Peirs, D. Van Neck, and M. Waroquier, Int. J. Quantum Chem. **91**, 113 (2003).
[18] K. Peirs, D. Van Neck, and M. Waroquier, J. Chem. Phys. **117**, 4095 (2002).
[19] C.O. Almbladh and A.C. Pedroza, Phys. Rev. A **29**, 2322 (1984).
[20] A.C. Pedroza, Phys. Rev. A **33**, 804 (1986).
[21] F. Aryasetiawan and M.J. Stott, Phys. Rev. B **38**, 2974 (1988).
[22] A. Görling, Phys. Rev. A **46**, 3753 (1992).
[23] A. Görling and M. Ernzerhof, Phys. Rev. A **51**, 4501 (1995).
[24] Y. Wang and R.G. Parr, Phys. Rev. A **47**, R1591 (1993).
[25] R. van Leeuwen and E.J. Baerends, Phys. Rev. A **49**, 2421 (1994).
[26] O.V. Gritsenko, R. van Leeuwen, and E.J. Baerends, Phys. Rev. A **52**, 1870 (1995).
[27] P.R.T. Schipper, O.V. Gritsenko, and E.J. Baerends, Theor. Chem. Acc. **98**, 16 (1997).
[28] Q. Zhao, R.C. Morrison, and R.G. Parr, Phys. Rev. A **50**, 2138 (1994).
[29] A.I. Al-Sharif, A. Qteish, and R. Resta, Phys. Rev. A **60**, 3541 (1999).
[30] F.A. Hamprecht, A.J. Cohen, D.J. Tozer, and N.C. Handy, J. Chem. Phys. **109**, 6264 (1998).
[31] C.-O. Almbladh and U. von Barth, Phys. Rev. B **31**, 3231 (1985).
[32] E. Engel and R.M. Dreizler, J. Comput. Chem. **20**, 31 (1999).
[33] C. Filippi, X. Gonze, and C. J. Umrigar, in *Recent Developments and Applications of Density Functional Theory*, edited by J. M. Seminario (Elsevier, Amsterdam, 1996).
[34] C.J. Umrigar and X. Gonze, Phys. Rev. A **50**, 3827 (1994).
[35] C. J. Umrigar and X. Gonze, in *High Performance Computing and its Application to the Physical Sciences*, Proceedings of the Mardi Gras '93 Conference, edited by D. A. Browne *et al.* (World Scientific, Singapore, 1993).
[36] C. Filippi, C.J. Umrigar, and X. Gonze, J. Chem. Phys. **107**, 9994 (1997).
[37] A. Savin, C.J. Umrigar, and X. Gonze, Chem. Phys. Lett. **288**, 391 (1998).
[38] A.I. Al-Sharif, R. Resta, and C.J. Umrigar, Phys. Rev. A **57**, 2466 (1998).
[39] X. Gonze (private communication).
[40] R.C. Morrison and Q. Zhao, Phys. Rev. A **51**, 1980 (1995).
[41] W.L. Luken and D.N. Beratan, Theor. Chem. Acc. **61**, 265 (1982).
[42] V.W. Maslen, Proc. Phys. Soc., London, Sect. A **69**, 734 (1956).
[43] G. Sperber, Int. J. Quantum Chem. **6**, 881 (1972).
[44] J.P. Perdew, R.G. Parr, M. Levy, and J.L. Balduz, Jr., Phys. Rev. Lett. **49**, 1691 (1982).
[45] J.P. Perdew and M.R. Norman, Phys. Rev. B **26**, 5445 (1982).
[46] L.A. Curtiss *et al.*, J. Chem. Phys. **114**, 9287 (2001).
[47] D.J. Tozer and N.C. Handy, J. Phys. Chem. A **102**, 3162 (1998).
[48] N.C. Handy and D.J. Tozer, Mol. Phys. **94**, 707 (1998).
[49] J.P. Perdew and K. Burke, Int. J. Quantum Chem. **57**, 309 (1996).